JACS
JOURNAL OF THE AMERICAN CHEMICAL SOCIETY
pubs.acs.org/JACS
Communication

Synthesis of Cyclo[18]carbon via Debromination of $C_{18}Br_6$

Lorel M. Scriven,[‖] Katharina Kaiser,[‖] Fabian Schulz, Alistair J. Sterling, Steffen L. Woltering, Przemyslaw Gawel, Kirsten E. Christensen, Harry L. Anderson,* and Leo Gross*

Cite This: J. Am. Chem. Soc. 2020, 142, 12921−12924
Read Online
ACCESS | Metrics & More | Article Recommendations | Supporting Information

ABSTRACT: Cyclo[18]carbon (C_{18}, a molecular carbon allotrope) can be synthesized by dehalogenation of a bromocyclocarbon precursor, $C_{18}Br_6$, in 64% yield, by atomic manipulation on a sodium chloride bilayer on Cu(111) at 5 K, and imaged by high-resolution atomic force microscopy. This method of generating C_{18} gives a higher yield than that reported previously from the cyclocarbon oxide $C_{24}O_6$. The experimental images of C_{18} were compared with simulated images for four theoretical model geometries, including possible bond-angle alternation: D_{18h} cumulene, D_{9h} polyyne, D_{9h} cumulene, and C_{9h} polyyne. Cumulenic structures, with (D_{9h}) and without (D_{18h}) bond-angle alternation, can be excluded. Polyynic structures, with (C_{9h}) and without (D_{9h}) bond-angle alternation, both show a good agreement with the experiment and are challenging to differentiate.

Synthetic carbon-rich materials and new carbon allotropes have attracted much attention over the past half century.[1] Allotropes based on two-coordinate *sp*-hybridized carbon are much more elusive than those based on trigonal sp^2-hybridized carbon.[2] Recently, we reported the synthesis of cyclo[18]-carbon, by elimination of carbon monoxide from $C_{24}O_6$ on bilayer sodium chloride on Cu(111) at 5 K, and we characterized this molecular carbon allotrope by high resolution atomic force microscopy (AFM).[3] Molecules of C_{18} showed a 9-fold symmetry, indicating a polyyne structure. However, many questions remain unanswered about the structure and properties of cyclo[*n*]carbons.[4,5] Second-order Jahn−Teller effects have been proposed to cause both bond-length alternation (BLA) and bond-angle alternation (BAA) in these homoatomic rings,[4,6−9] whereas Hückel aromaticity should favor a high-symmetry structure in C_n rings with $n = 4m + 2$, such as C_{18}.[10] Theoretical studies have suggested four possible geometries for C_{18}: D_{18h} cumulene, D_{9h} polyyne, D_{9h} cumulene, and C_{9h} polyyne (**A**−**D**, Figure 1a−d).[4,6−9] Here we report a study of C_{18} synthesized via a new route: dehalogenation of $C_{18}Br_6$, which occurs under milder conditions, and in five times higher yield (64%) compared to the yield of formation from $C_{24}O_6$ (13%). The dissociated Br atoms are immobile on the NaCl surface under our imaging conditions and hinder motion of the C_{18} molecules, which facilitated high-resolution AFM imaging at different tip heights. We compared the AFM data for C_{18} with simulated images for structures **A**−**D**, using different bond lengths (d_1 and d_2) and different bond angles (θ_1 and θ_2). The results show that the cumulenic D_{18h} and D_{9h} geometries can be excluded, while both the polyyne geometries, D_{9h} and C_{9h}, are consistent with the experimental images.

The bromocyclocarbon precursor, $C_{18}Br_6$, was synthesized as shown in Scheme 1. *Syn*-selective diboration of the central C≡C triple bond of bis(triisopropylsilyl)hexatriyne **1**, using a platinum-catalyzed reaction developed by Suzuki et al.,[11] proceeded cleanly to give the (*Z*)-bis(boryl)enediyne **2**. This

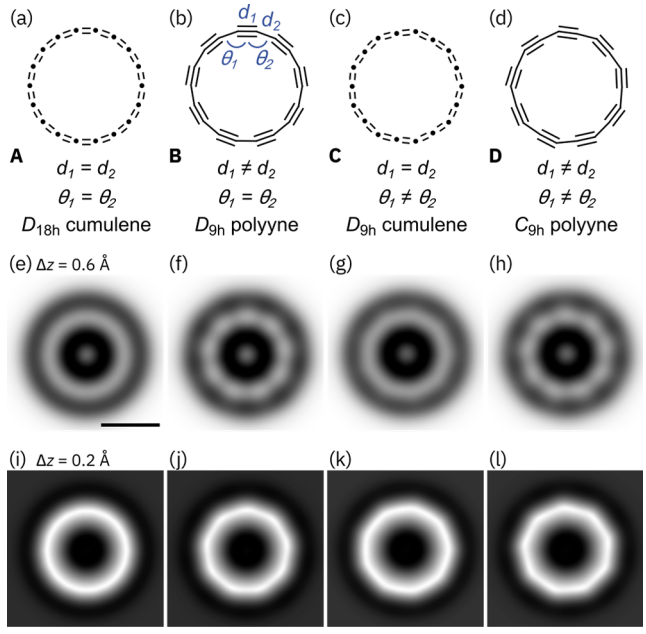

Figure 1. Possible geometries of cyclo[18]carbon, **A**−**D**, together with respective simulated AFM images at two different tip−sample distances, (e)−(h): Δz = 0.6 Å; (i)−(l): Δz = 0.2 Å. The AFM simulations correspond to geometries with **A**: $d_1 = d_2 = 1.30$ Å, $\theta_1 = \theta_2 = 160°$; **B**: $d_1 = 1.38$ Å, $d_2 = 1.24$ Å, $\theta_1 = \theta_2 = 160°$; **C**: $d_1 = d_2 = 1.30$ Å, $\theta_1 = 171.4°$, $\theta_2 = 148.6°$; **D**: $d_1 = 1.38$ Å, $d_2 = 1.24$ Å, $\theta_1 = 173.1°$, $\theta_2 = 146.9°$. The scale bar in (e) is 5 Å and applies to all simulated AFM images.

Received: May 7, 2020
Published: July 10, 2020

https://dx.doi.org/10.1021/jacs.0c05033
J. Am. Chem. Soc. 2020, 142, 12921−12924

Scheme 1. Synthesis of Cyclo[18]carbon *via* $C_{18}Br_6$

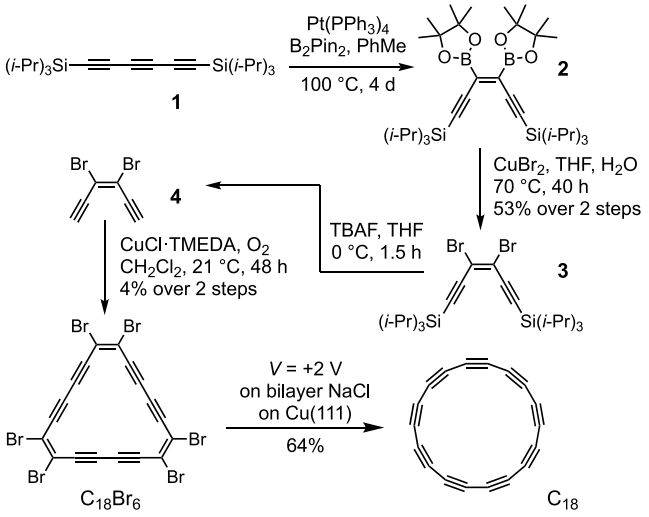

intermediate was stereoselectively bromodeboronated using copper(II) bromide, to yield the TIPS-protected (*Z*)-dibromo-enediyne **3**, in 53% yield over two steps, which was deprotected using tetrabutylammonium fluoride (TBAF) to yield (*Z*)-dibromo-enediyne **4**. This enediyne is unstable in the pure form and must be handled as a solution. Oxidative cyclo-oligomerization of **4** under catalytic Glaser–Hay conditions[12] (CuCl·TMEDA, 0.2 equiv) gave $C_{18}Br_6$ in 4% yield over two steps as a bright red, sparingly soluble, crystalline solid. Other cyclic oligomers, $C_{12}Br_4$ and $C_{24}Br_8$, were also tentatively detected in the reaction mixture, but have not yet been isolated.

$C_{18}Br_6$ is stable under ambient conditions, in solution, and in the solid state, with no significant decomposition over several days at room temperature, and the solid can be stored for weeks at −20 °C. However, it is a shock-sensitive explosive (e.g., it explodes when scratched with a spatula) and care was taken to work on a small scale. Differential scanning calorimetry showed that $C_{18}Br_6$ undergoes exothermic decomposition at 85–125 °C (ΔH = −109 kJ/mol). $C_{18}Br_6$ is almost insoluble in most organic solvents but sparingly soluble in carbon disulfide. Single crystals suitable for X-ray analysis were grown from a saturated solution of $C_{18}Br_6$ in CS_2 at 4 °C (Figure 2). The crystals are orthorhombic with eight molecules per unit cell, and half a molecule of $C_{18}Br_6$ in the asymmetric unit. The compound adopts a layer structure, with a layer spacing of 3.412(1) Å, and the packing arrangement resembles that in the corresponding hydrocarbon, $C_{18}H_6$.[13]

The synthesis and characterization of C_{18} was carried out in a low-temperature combined STM/AFM system (for more details, see Supporting Information). The $C_{18}Br_6$ precursor was thermally sublimed onto a cold Cu(111) surface ($T \approx 5$ K) partially covered with NaCl bilayer islands, yielding a submonolayer coverage of well-dispersed molecules. No intact $C_{18}Br_6$ molecules were observed on the bare Cu(111) surface, possibly due to its high reactivity, and all atom-manipulation experiments were carried out on bilayer NaCl. The tip was functionalized with carbon monoxide (CO) to enhance the AFM contrast.[14,15] AFM measurements were recorded in constant-height mode, where Δz denotes the tip height offset with respect to the STM set point (positive Δz corresponds to an increase in tip–sample distance).

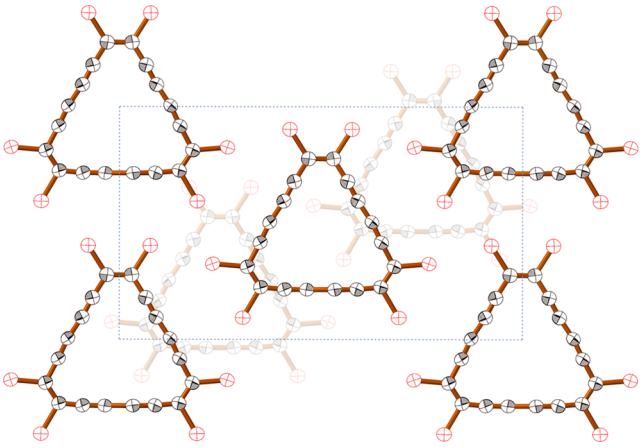

Figure 2. Crystal structure of $C_{18}Br_6$, viewed along the crystallographic *b*-axis, showing two layers of molecules. The central rectangle is the unit cell. (Thermal ellipsoids: 50% probability level.)

Sublimation of $C_{18}Br_6$ onto bilayer NaCl yielded almost exclusively intact $C_{18}Br_6$ molecules with no appearance of C_{18}. A small fraction of the molecules (less than 5%) appeared to be missing one of the six Br atoms. This indicates that, unlike the cyclocarbon oxide precursor $C_{24}O_6$,[3] no significant unmasking occurs during sublimation and adsorption. Figure 3a–d show

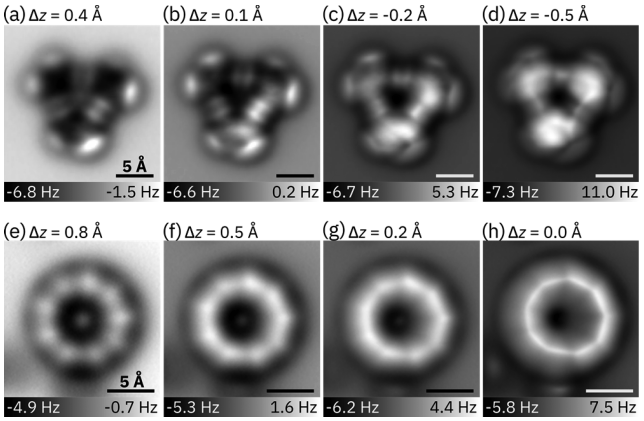

Figure 3. AFM images of (a)–(d) $C_{18}Br_6$ and (e)–(h) cyclo[18]carbon recorded at different Δz. In (e)–(h), the scan angle was adjusted such that the scanned plane was parallel to the molecule instead of the underlying surface. Δz denotes the difference in tip–sample distance with respect to the set point of I = 0.5 pA, V = 0.2 V. All scale bars 5 Å.

AFM images of the intact $C_{18}Br_6$ precursor recorded at different tip–sample distances, revealing a characteristic triangular shape. The six bright features at the corners relate to the Br atoms and the bright features along the edges of the triangular core correspond to C≡C triple bonds.[3,16,17] The nonuniform brightness of Br atoms and triple bonds within the molecule results from a nonplanar adsorption geometry, with the brighter parts of the molecule indicating their greater height.[18] These differences are most distinct in the AFM images recorded at large tip–sample distances (Figure 3a,b). At small tip–sample distances (Figure 3c,d), tip relaxations, such as tilting of the CO, cause image distortions, which lead to apparent sharpening of the bonds[15,19] and facilitate bond-order discrimination.[19,20]

https://dx.doi.org/10.1021/jacs.0c05033
J. Am. Chem. Soc. 2020, 142, 12921–12924

Debromination of $C_{18}Br_6$ was achieved by positioning the tip at a lateral distance of 1−3 nm from the center of the molecule, retracting it by 2−3 Å from the STM set point (typically I = 0.5 pA, V = 0.2 V) to minimize the tunneling current (I < 50 fA) and increasing the bias voltage to 2 V for up to 5 s. With this procedure, we could remove one to six bromine atoms and ultimately generate cyclo[18]carbon from $C_{18}Br_6$ in a yield of ∼64% (for details on the statistics and the process, see the Supporting Information, Sections 6 and 7). Thus, cyclo[18]carbon could be generated more reliably and in higher yield than in previous work, from a cyclocarbon oxide precursor.[3] The increased yield of formation of cyclo[18]-carbon is probably a consequence of the lower voltage required for unmasking. AFM images of cyclo[18]carbon synthesized from $C_{18}Br_6$ were recorded at several different tip−sample distances (Figure 3e−h). Cyclo[18]carbon adsorbs in a nonplanar geometry on bilayer NaCl.[3] The plane for constant-height imaging was adjusted by 4° with respect to the NaCl surface to tilt the imaging plane approximately parallel to the molecular plane, so as to obtain a uniform contrast across the molecule. The dark features next to the cyclo[18]carbon molecule in Figure 3e (bottom and left), which become bright in Figure 3h, can be assigned to the dissociated bromine atoms. These dissociated Br atoms were found to stabilize and prevent motion of the cyclo[18]carbon molecules (see also Figures S3 and S4, Supporting Information), which is advantageous for high-resolution AFM imaging: it enabled us to obtain AFM data for C_{18} with improved resolution and data sets with different tip heights on the same molecule without moving it (Figure 3e−h).

As reported for cyclo[18]carbon formed from $C_{24}O_6$, the molecule shows nine bright lobes in the AFM images recorded at larger tip−sample distances (Figure 3e,f) that transition into nine corners for smaller tip−sample distances (Figure 3g,h). The nine bright lobes are assigned to the triple bonds. The experimental AFM images of C_{18} (Figure 3e−h) were compared with simulated images of C_{18} using the probe particle model[15] based on model geometries **A**−**D** with different degrees of BLA and BAA. Bond lengths and bond angles were adopted from previously published high level *ab initio* CCSD theory calculations with the cc-pVDZ basis set (C_{18h} cumulene: $d_1 = d_2$ = 1.30 Å, $\theta_1 = \theta_2$ = 160°; D_{9h} polyyne: d_1 = 1.38 Å, d_2 = 1.24 Å, $\theta_1 = \theta_2$ = 160°; D_{9h} cumulene: $d_1 = d_2$ = 1.30 Å, θ_1 = 157.2°, θ_2 = 162.9°; C_{9h} polyyne: d_1 = 1.38 Å, d_2 = 1.24 Å, θ_1 = 156.7°, θ_2 = 163.3°).[9] The differences in BLA between the cumulenic and polyynic structures produce distinct changes in the simulated images, while differences in BAA lead to less pronounced changes (Figure 1e−l and Supporting Information, Figures S6−S9). To observe the effect of BAA on the AFM contrast and to test whether larger BAA in the D_{9h} cumulene and C_{9h} polyyne would allow a better distinction from the C_{18h} cumulene and D_{9h} polyyne, respectively, we increased the amount of BAA by up to a factor of 4 compared to the theoretically predicted values (see Supporting Information, Figures S6−S9). Figure 1e−l shows simulated AFM images at two different tip−sample distances for the optimized D_{18h} cumulene and D_{9h} polyyne geometries, as well as the D_{9h} cumulene and C_{9h} polyyne with four times the calculated BAA of ref 9 (**C**: θ_1 = 171.4°, θ_2 = 148.6°; **D**: θ_1 = 173.1°, θ_2 = 146.9°). BAA strongly affects the simulated contrast of the D_{9h} cumulene for small tip heights (Figure 1k), and the contrast of the cumulene with large BAA becomes very similar to those of the polyynes (Figure 1j,l), showing a characteristic nonagon. The corners of the D_{9h} cumulene are located above atom positions, while the corners of the D_{9h} polyyne are above triple bonds (see Supporting Information). Importantly, the polyyne models can be distinguished from both cumulene models at larger tip height (see Figure 1e,g); only the polyynes exhibit nine bright lobes (Figure 1f,h) in agreement with the experiment (Figure 3e,f). Thus, both cumulenic geometries of cyclo[18]carbon (D_{18h} and D_{9h}) can be excluded. However, the polyyne geometries (D_{9h} and C_{9h}) show almost no change in contrast variations as we varied the BAA, which implies that for the polyyne geometries it is challenging to resolve or quantify the extent of BAA from AFM images. Two factors may contribute to this effect: (i) In the cumulenic geometries, the introduction of BAA corresponds to a significant change in symmetry from D_{18h} to D_{9h} (i.e., from 18-fold to 9-fold symmetry). However, in the polyyne geometries, the introduction of BAA corresponds to a more subtle change in symmetry from D_{9h} to C_{9h}, both of which are 9-fold symmetric. (ii) The AFM contrast of the polyynic geometries is dominated by strong modulations around the carbon ring, due to the large differences in the electron density between triple and single bonds, which are enhanced in AFM by relaxations of the CO tip.[19] On the other hand, BAA affects the position and orientation of the bonds without causing large changes in the electron densities of bonds, resulting in relatively subtle contrast modulations.

In conclusion, C_{18} is generated by debromination of $C_{18}Br_6$ on bilayer NaCl on Cu(111) at 5 K, with a five times greater yield than from $C_{24}O_6$ precursors. AFM simulations of different geometries of C_{18} showed that BAA can have a considerable effect on the simulated AFM images for the cumulenic structure but is barely visible for the polyyne. The simulations confirm that the cumulene geometries, even those with extreme BAA, can be excluded, corroborating the polyynic structure of C_{18} on NaCl. However, it is challenging to rule out or quantify BAA in the polyynic geometry. Interaction with the surface may affect the molecular structure, and the structure of C_{18} in vacuum might be different from that on NaCl.[5a] Our results indicate that debromination of cyclocarbon precursors is a promising route to explore also other cyclo[n]carbons by on-surface chemistry.

■ ASSOCIATED CONTENT

Supporting Information

The Supporting Information is available free of charge at https://pubs.acs.org/doi/10.1021/jacs.0c05033.

Details of synthetic protocols, DSC analysis, crystallography, scanning probe microscopy, reaction statistics, AFM simulations and selected spectra (PDF)

Crystallographic data for $C_{18}Br_6$ (1998472) (CIF)

■ AUTHOR INFORMATION

Corresponding Authors

Leo Gross − *IBM Research−Zurich, 8803 Rüschlikon, Switzerland;* orcid.org/0000-0002-5337-4159; Email: lgr@zurich.ibm.com

Harry L. Anderson − *Department of Chemistry, Oxford University, Oxford OX1 3TA, U.K.;* orcid.org/0000-0002-1801-8132; Email: harry.anderson@chem.ox.ac.uk

Authors

Lorel M. Scriven − *Department of Chemistry, Oxford University, Oxford OX1 3TA, U.K.;* orcid.org/0000-0002-7367-2946

Katharina Kaiser − *IBM Research−Zurich, 8803 Rüschlikon, Switzerland;* orcid.org/0000-0001-7519-8005

Fabian Schulz − *IBM Research−Zurich, 8803 Rüschlikon, Switzerland;* orcid.org/0000-0002-1359-4675

Alistair J. Sterling − *Department of Chemistry, Oxford University, Oxford OX1 3TA, U.K.;* orcid.org/0000-0002-3571-1094

Steffen L. Woltering − *Department of Chemistry, Oxford University, Oxford OX1 3TA, U.K.;* orcid.org/0000-0002-9697-9019

Przemyslaw Gawel − *Department of Chemistry, Oxford University, Oxford OX1 3TA, U.K.*

Kirsten E. Christensen − *Department of Chemistry, Oxford University, Oxford OX1 3TA, U.K.*

Complete contact information is available at: https://pubs.acs.org/10.1021/jacs.0c05033

Author Contributions

[‖]L.M.S. and K.K. contributed equally.

Notes

The authors declare no competing financial interest.

■ ACKNOWLEDGMENTS

We thank the ERC (Grants 320869 and 682144) and the Leverhulme Trust (Project Grant RPG-2017-032) for support. A.J.S. thanks the EPSRC and the Oxford-Radcliffe Scholarship for support (EP/L015838/1) and for access to the Dirac cluster at Oxford (EP/L015722/1). P.G. acknowledges a Postdoc.Mobility fellowship from the Swiss National Science Foundation (P300P2_177829). We thank Fernanda Duarte, Rolf Allenspach, Shadi Fatayer, and Florian Albrecht for discussions.

■ REFERENCES

(1) (a) Krätschmer, W.; Lamb, L. D.; Fostiropoulos, K.; Huffman, D. R. Solid C_{60}: A New Form of Carbon. *Nature* **1990**, *347*, 354−358. (b) Kroto, H. W. C_{60}: Buckminsterfullerene, The Celestial Sphere that Fell to Earth. *Angew. Chem., Int. Ed. Engl.* **1992**, *31*, 111−129. (c) Iijima, S.; Ichihashi, T. Single-Shell Carbon Nanotubes of 1-nm Diameter. *Nature* **1993**, *363*, 603−605. (d) Novoselov, K. S.; Geim, A. K.; Morozov, S. V.; Jiang, D.; Zhang, Y.; Dubonos, S. V.; Grigorieva, I. V.; Firsov, A. A. Electric Field Effect in Atomically Thin Carbon Films. *Science* **2004**, *306*, 666−669. (e) Kinloch, I. A.; Suhr, J.; Lou, J.; Young, R. J.; Ajayan, P. M. Composites with Carbon Nanotubes and Graphene: An Outlook. *Science* **2018**, *362*, 547−553.

(2) (a) Diederich, F. Carbon Scaffolding - Building Acetylenic All-Carbon and Carbon-Rich Compounds. *Nature* **1994**, *369*, 199−207. (b) Diederich, F.; Kivala, M. All-Carbon Scaffolds by Rational Design. *Adv. Mater.* **2010**, *22*, 803−812.

(3) Kaiser, K.; Scriven, L. M.; Schulz, F.; Gawel, P.; Gross, L.; Anderson, H. L. An sp-Hybridized Molecular Carbon Allotrope, Cyclo[18]carbon. *Science* **2019**, *365*, 1299−1301.

(4) Nandi, A.; Solel, E.; Kozuch, S. Carbon Tunneling in the Automerization of Cyclo[18]carbon. *Chem. - Eur. J.* **2020**, *26*, 625−628.

(5) (a) Baryshnikov, G. V.; Valiev, R. R.; Kuklin, A. V.; Sundholm, D.; Ågren, H. Cyclo[18]carbon: Insight into Electronic Structure, Aromaticity, and Surface Coupling. *J. Phys. Chem. Lett.* **2019**, *10*, 6701−6705. (b) Pereira, Z. S.; da Silva, E. Z. Spontaneous Symmetry Breaking in Cyclo[18]Carbon. *J. Phys. Chem. A* **2020**, *124*, 1152−1157. (c) Stasyuk, A. J.; Stasyuk, O. A.; Solà, M.; Voityuk, A. A. Cyclo[18]carbon: the smallest all-carbon electron acceptor. *Chem. Commun.* **2020**, *56*, 352−355. (d) Hussain, S.; Chen, H.; Zhang, Z.; Zheng, H. Vibrational spectra and chemical imaging of cyclo[18] carbon by tip enhanced Raman spectroscopy. *Chem. Commun.* **2020**, *56*, 2336−2339.

(6) Parasuk, V.; Almlöf, J.; Feyereisen, M. W. The [18] All-Carbon Molecule: Cumulene or Polyacetylene? *J. Am. Chem. Soc.* **1991**, *113*, 1049−1050.

(7) Plattner, D. A.; Houk, K. N. C_{18} Is a Polyyne. *J. Am. Chem. Soc.* **1995**, *117*, 4405−4406.

(8) Torelli, T.; Mitas, L. Electron Correlation in C_{4N+2} Carbon Rings: Aromatic versus Dimerized Structures. *Phys. Rev. Lett.* **2000**, *85*, 1702−1705.

(9) Arulmozhiraja, S.; Ohno, T. CCSD Calculations on C_{14}, C_{18}, and C_{22} Carbon Clusters. *J. Chem. Phys.* **2008**, *128*, 114301.

(10) (a) Diederich, F.; Rubin, Y.; Knobler, C. B.; Whetten, R. L.; Schriver, K. E.; Houk, K. N.; Li, Y. All-Carbon Molecules: Evidence for the Generation of Cyclo[18]carbon from a Stable Organic Precursor. *Science* **1989**, *245*, 1088−1090. (b) Fowler, P. W.; Mizoguchi, N.; Bean, D. E.; Havenith, R. W. A. Double Aromaticity and Ring Currents in All-Carbon Rings. *Chem. - Eur. J.* **2009**, *15*, 6964−6972.

(11) Ishiyama, T.; Matsuda, N.; Miyaura, N.; Suzuki, A. Platinum-(0)-Catalyzed Diboration of Alkynes. *J. Am. Chem. Soc.* **1993**, *115*, 11018−11019.

(12) (a) Hay, A. S. Oxidative Coupling of Acetylenes. *J. Org. Chem.* **1962**, *27*, 3320−3321. (b) Jones, G. E.; Kendrick, D. A.; Holmes, A. B. 1,4-Bis(trimethylsilyl)buta-1,3-diyne. *Org. Synth.* **1987**, *65*, 52.

(13) (a) Suzuki, M.; Comito, A.; Khan, S. I.; Rubin, Y. Nanochannel Array within a Multilayered Network of a Planarized Dehydro[24]-annulene. *Org. Lett.* **2010**, *12*, 2346−2349. (b) Lungerich, D.; Nizovtsev, A. V.; Heinemann, F. W.; Hampel, F.; Meyer, K.; Majetich, G.; Schleyer, P. v. R.; Jux, N. [18]Annulene put into a new perspective. *Chem. Commun.* **2016**, *52*, 4710−4713.

(14) Gross, L.; Mohn, F.; Moll, N.; Liljeroth, P.; Meyer, G. The Chemical Structure of a Molecule Resolved by Atomic Force Microscopy. *Science* **2009**, *325*, 1110−1114.

(15) (a) Hapala, P.; Kichin, G.; Wagner, C.; Tautz, F. S.; Temirov, R.; Jelínek, P. Mechanism of High-Resolution STM/AFM Imaging with Functionalized Tips. *Phys. Rev. B: Condens. Matter Mater. Phys.* **2014**, *90*, 085421. (b) Hämäläinen, S. K.; van der Heijden, N.; van der Lit, J.; den Hartog, S.; Liljeroth, P.; Swart, I. Intermolecular Contrast in Atomic Force Microscopy Images without Intermolecular Bonds. *Phys. Rev. Lett.* **2014**, *113*, 186102.

(16) De Oteyza, D. G.; Gorman, P.; Chen, Y. C.; Wickenburg, S.; Riss, A.; Mowbray, D. J.; Etkin, G.; Pedramrazi, Z.; Tsai, H. Z.; Rubio, A.; Crommie, M. F.; Fischer, F. R. Direct Imaging of Covalent Bond Structure in Single-Molecule Chemical Reactions. *Science* **2013**, *340*, 1434−1437.

(17) Pavliček, N.; Gawel, P.; Kohn, D. R.; Majzik, Z.; Xiong, Y.; Meyer, G.; Anderson, H. L.; Gross, L. Polyyne Formation via Skeletal Rearrangement Induced by Atomic Manipulation. *Nat. Chem.* **2018**, *10*, 853−858.

(18) Schuler, B.; Liu, W.; Tkatchenko, A.; Moll, N.; Meyer, G.; Mistry, A.; Fox, D.; Gross, L. Adsorption Geometry Determination of Single Molecules by Atomic Force Microscopy. *Phys. Rev. Lett.* **2013**, *111*, 106103.

(19) Gross, L.; Mohn, F.; Moll, N.; Schuler, B.; Criado, A.; Guitián, E.; Peña, D.; Gourdon, A.; Meyer, G. Bond-Order Discrimination by Atomic Force Microscopy. *Science* **2012**, *337*, 1326−1329.

(20) Riss, A.; Wickenburg, S.; Gorman, P.; Tan, L. Z.; Tsai, H. Z.; De Oteyza, D. G.; Chen, Y. C.; Bradley, A. J.; Ugeda, M. M.; Etkin, G.; Louie, S. G.; Fischer, F. R.; Crommie, M. F. Local Electronic and Chemical Structure of Oligo-Acetylene Derivatives Formed through Radical Cyclizations at a Surface. *Nano Lett.* **2014**, *14*, 2251−2255.